Intrusive Gravity Currents

By S. J. D. D'Alessio, T. B. Moodie, J. P. Pascal, and G. E. Swaters

Intrusive gravity currents arise when a fluid of intermediate density intrudes into an ambient fluid. These intrusions may occur in both natural and human-made settings and may be the result of a sudden release of a fixed volume of fluid or the steady or time-dependent injection of such a fluid. In this article we analytically and numerically analyze intrusive gravity currents arising both from the sudden release of a fixed volume and the steady injection of fluid having a density that is intermediate between the densities of an upper layer bounded by a free surface and a heavier lower layer resting on a flat bottom. For the physical problems of interest we assume that the dynamics of the flow are dominated by a balance between inertial and buoyancy forces with viscous forces being negligible. The three-layer shallow-water equations used to model the two-dimensional flow regime include the effects of the surrounding fluid on the intrusive gravity current. These effects become more pronounced as the fraction of the total depth occupied by the intrusive current increases. To obtain some analytical information concerning the factors effecting bore formation we further reduce the complexity of our three-layer model by assuming small density differences among the different layers. This reduces the model equations from a 6×6 to a 4×4 system. The limit of applicability of this weakly stratified model for various ranges of density differences is examined numerically. Numerical results, in most instances, are

Address for correspondence: Professor T. B. Moodie, Applied Mathematics Institute, Department of Mathematical Sciences, University of Alberta, Edmonton, Alberta T6G 2G1 Canada.

STUDIES IN APPLIED MATHEMATICS 98:19–46

Published by Blackwell Publishers, 350 Main Street, Malden, MA 02148, USA, and 108 Cowley Road, Oxford, OX4 1JF, UK.

obtained using MacCormack's method. It is found that the intrusive gravity current displays a wide range of flow behavior and that this behavior is a strong function of the fractional depth occupied by the release volume and any asymmetries in the density differences among the various layers. For example, in the initially symmetric sudden release problem it is found that an interior bore does not form when the fractional depth of the release volume is equal to or less than 50% of the total depth. The numerical simulations of fixed-volume releases of the intermediate layer for various density and initial depth ratios demonstrate that the intermediate layer quickly slumps from any isostatically uncompensated state to its Archimedean level thereby creating a wave of opposite sign ahead of the intrusion on the interface between the upper and lower layers. Similarity solutions are obtained for several cases that include both steady injection and sudden releases and these are in agreement with the numerical solutions of the shallow-water equations. The 4×4 weak stratification system is also subjected to a wavefront analysis to determine conditions for the initiation of leading-edge bores. These results also appear to be in agreement with numerical solutions of the shallow-water equations.

1. Introduction

A gravity current consists of a tongue of fluid intruding laterally into an ambient body of fluid when this motion is driven by density differences [1]. We employ the term "intrusive" gravity current strictly for currents that appear at an intermediate level to distinguish them from either top or bottom gravity flows. Gravity currents play an important role in many known natural phenomena and will likely be seen to figure prominently in other natural events as our level of understanding of them is increased. In particular a clear understanding of the dynamics of the flow, including bore formation, is important if we are to quantify the flow's ability to influence its surroundings [1–3].

One of the earliest theoretical calculations in the area of gravity currents was by von Kármán [4]. Considering steady currents he provided a mathematical demonstration to show that a current of density ρ_2 and depth h propagates under a fluid of density ρ_1 ($< \rho_2$) and of semi-infinite depth at a speed c, where

$$c = (2g'h)^{1/2}, \tag{1.1}$$

and the reduced gravity is defined by $g' \equiv g(\rho_2 - \rho_1)/\rho_1$, where g is the acceleration due to gravity. Benjamin [5], in what now has become a classic of the gravity current literature, subsequently explained that von Kármán's reasoning in arriving at (1.1) was flawed but that the result, for this restricted problem, was nevertheless true. Benjamin [5] studied steady irrotational gravity currents in perfect fluids having a fixed upper boundary by regarding

the overall balance to be between horizontal momentum and the hydrostatic force. Using this simple model he was able to achieve broad agreement with the earlier experiments of Keulegan [6]. The majority of the theoretical work on gravity currents from the time of von Kármán up to Benjamin and right on through into the mid-1980s treated the gravity current as steady, existing in either an inertia-buoyancy balance or, at later stages in the flow, in a viscous-buoyancy balance and finally, in the very late stages of the flow, a viscous-surface tension balance. A notable exception was the work of Hoult [7] in which governing equations were established and subsequently solved rather than seeking a time-independent force balance. His formulation for bottom flows has the advantage over that of Huppert [8] in that it includes the effects of motion of the lighter upper fluid, a requirement when the depth of the bottom current is comparable to the depth of the overlying fluid [2]. Hoult's solution (and that of Huppert [8]) was obtained in terms of a similarity variable and so the derived relationships are valid only after sufficient time has elapsed since release for the initial geometry to be irrelevant.

Further in the realm of time-dependent gravity flow studies is the work of Rottman and Simpson [9] on instantaneous releases of bottom gravity flows. Their detailed experiments studied instantaneous releases for $0 < h_0/H \leq 1$ concentrating on the flow's transition to the self-similar phase, where h_0 is the initial depth of the released fluid and H the total depth of the fluid in the channel. One of the key features of their observations was that for h_0/H equal to or slightly less than unity the disturbance generated at the endwall has the appearance of an internal hydraulic drop and for smaller values of h_0/H it is a long wave of depression. These experiments serve to emphasize the importance of including the effect of the ambient fluid on the gravity current when that current is a sensible fraction of the total depth. As a framework for discussing these experiments they solved an initial value problem for the two-layer, shallow-water, rigid lid, Boussinesq equations using the method of characteristics. Their interpretation of the experimental results in terms of the numerical simulations gives, at best, a qualitative understanding for $0 < h_0/H < \frac{1}{2}$. However, for $h_0/H > \frac{1}{2}$ there is little resemblance between their numerical simulations and the experimentally observed transition of the flow to the self-similar phase. D'Alessio et al. [10] employed a two-layer shallow-water model to study sudden releases for fixed volumes into an ambient fluid. Using MacCormack's method for numerical integration of the hyperbolic system they were able to achieve good agreement with the experimental results for transition to self-similarity. This agreement is evidenced by comparing the results of Figure 9 in D'Alessio et al. [10] with the experimental results in Figure 8 of Rottman and Simpson [9]. The experimentally observed slowing down of the front as the rear bore overtakes it is captured by the model in D'Alessio et al. [10]. Grundy and Rottman [11] in their study of the approach to self-similarity for solutions to the shallow-water equations

for sudden releases employed a set of model equations that ignored inertial effects due to the presence of the ambient fluid. Their subsequent numerical studies for plane flow show little resemblance to the observed flows of Rottman and Simpson [9].

In this article we analyze fully time-dependent intrusive gravity flows using a three-layer shallow-water model. We are able to provide compelling evidence to show that the creation of internal hydraulic jumps requires vigorous backflow in the surrounding fluids thereby showing that to model the transition to self-similarity observed in flows it is necessary to take the surrounding fluids into account by means of finite thickness layers. We are also able to point out that intrusion models based on the shallow-water equations may lose hyperbolicity for sufficiently high Froude numbers thereby causing the numerical scheme to break down. Using the method of wavefront expansions we are able to obtain analytical results, relating to shock formation in the three-layer model, that confirm our numerical results. These analytical results also point out that the characteristic field can have local linear degeneracies that prevent shock formation at the front.

The ideas and methods employed in this article are an extension of those used previously [10] and are delineated in Section 2, where the model equations, boundary conditions, and initial conditions are presented. Section 3 is then devoted to numerical studies, their interpretation, and a brief investigation of similarity solutions and their comparison to numerical solutions of the shallow-water equations. In Section 4 we employ a wavefront analysis to explore conditions for the formation of interior bores at the interface between two fluids in our three-layer model. Section 5 is devoted to a brief discussion of results.

2. Formulation of the model

In Figure 1, $\eta(x, t)$ represents the displacement of the free surface from its undisturbed configuration, $u_1(x, t)$, $u_2(x, t)$, and $u_3(x, t)$ are the x-components of velocity in the upper, intermediate, and lower layers, respectively, and $h_2(x, t)$ and $h_3(x, t)$ give the location of the upper surfaces of the intermediate and lower layers, respectively. The locations marked on the axes of Figure 1 are related to the initial conditions for the sudden release of the fixed volume in that at $t = 0$ we prescribe the conditions

$$h_3 = \begin{cases} h_{3_0}, & x \le x_0, \\ H_0, & x > x_0, \end{cases} \qquad \text{and} \qquad h_2 = \begin{cases} h_{2_0}, & x \le x_0, \\ H_0, & x > x_0. \end{cases} \tag{2.1}$$

The total mean depth is represented by H, while ρ_1, ρ_2, and ρ_3 ($\rho_3 > \rho_2 > \rho_1$; stable stratification) represent the constant densities of the three homogeneous fluid layers.

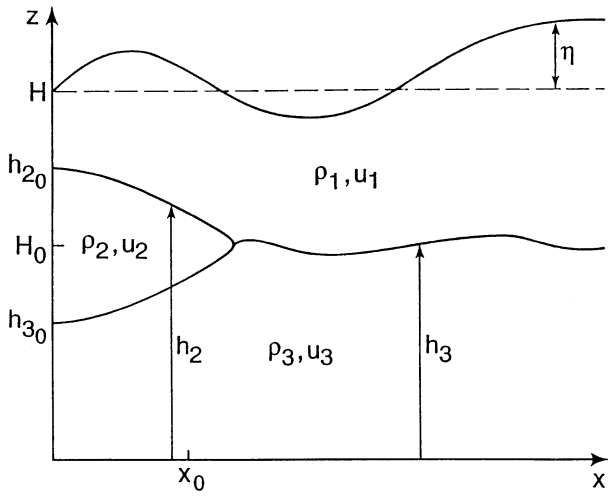

Figure 1. A sketch of the three-layer model for intrusive gravity currents.

The initial flow following the release of a gravity current is most often a highly complex one. However, soon after release the current has spread to such an extent that its length is very much greater than its vertical dimension, which is slowly varying over the horizontal position x and in time t [2]. For such conditions it is reasonable to neglect vertical gradients in the dynamic pressure and to assume a hydrostatic pressure distribution [12]. We also assume that the Reynolds number of the flow is sufficiently high that viscous forces are negligible and we neglect the effects of surface tension and assume that there is no mixing between layers.

All of the above assumptions lead us to represent the three-layer model for gravity flows in terms of shallow-water theory whose governing equations are

$$\frac{\partial u_1}{\partial t} + \frac{\partial}{\partial x}\left(\frac{1}{2}\,u_1^2 + \eta\right) = 0, \tag{2.2}$$

$$\frac{\partial}{\partial t}\left(\frac{g_1'}{g}\,\eta - h_2\right) + \frac{\partial}{\partial x}\left[\left(1 + \frac{g_1'}{g}\,\eta - h_2\right)u_1\right] = 0, \tag{2.3}$$

$$\frac{\partial u_2}{\partial t} + \frac{\partial}{\partial x}\left[\frac{1}{2}\,u_2^2 + h_2 + \left(1 - \frac{g_1'}{g}\right)\eta\right] = 0, \tag{2.4}$$

$$\frac{\partial}{\partial t}\,(h_2 - h_3) + \frac{\partial}{\partial x}\,[(h_2 - h_3)u_2] = 0, \tag{2.5}$$

$$\frac{\partial u_3}{\partial t} + \frac{\partial}{\partial x}\left[\frac{1}{2}\,u_3^2 + \frac{g_2'}{g_1'}\,h_3 + \left(\frac{g_3' - g_2'}{g_1'}\right)h_2 + \left(1 - \frac{g_3'}{g}\right)\eta\right] = 0, \tag{2.6}$$

$$\frac{\partial h_3}{\partial t} + \frac{\partial}{\partial x}\,(h_3 u_3) = 0. \tag{2.7}$$

These equations are in nondimensional form and satisfy the usual kinematic conditions at the free surface and the interfaces with closure being achieved by invoking continuity of pressure between the bottom and intermediate layers. In these equations g is the acceleration due to gravity and g'_n $(n = 1, 2, 3)$ are reduced gravities defined by

$$g'_1 \equiv \frac{\rho_2 - \rho_1}{\rho_2}\, g, \qquad g'_2 \equiv \frac{\rho_3 - \rho_2}{\rho_3}\, g, \qquad g'_3 \equiv \frac{\rho_3 - \rho_1}{\rho_3}\, g. \tag{2.8}$$

The system (2.2)–(2.7) was rendered nondimensional by employing a scaling that focuses on the nonlinear internal gravity wave processes thereby "filtering" out surface wave phenomena. Since the phase/group speeds for internal gravity waves are smaller than those for surface gravity waves (assuming relatively small reduced gravity), we may alternatively view this approximation as a low-frequency approximation that filters out the high frequencies. The nondimensional quantities are related to their dimensional counterparts by

$$\begin{gathered}(\widetilde{u}_1, \widetilde{u}_2, \widetilde{u}_3) = (u_1, u_2, u_3)(g'_1 H)^{1/2}, \\ \widetilde{h}_2 = H h_2, \qquad \widetilde{h}_3 = H h_3, \qquad \widetilde{\eta} = g'_1 H \eta / g, \\ L/T = (g'_1 H)^{1/2},\end{gathered} \tag{2.9}$$

where L is a horizontal length scale and T a time scale, which are chosen so that their ratio gives $(g'_1 H)^{1/2}$ and dimensional quantities are signified by a tilde.

The physical problems considered in this article correspond to the sudden release of a fixed volume of fluid, initially at rest, having a density that is intermediate between that of the top layer and bottom layer as well as the steady injection of such a fluid. In both cases initial value problems for the system of equations are to be posed and solved. It is assumed that a solid boundary is located at $x = 0$ and that the fluid remains undisturbed at large distances. For the sudden release problem the initial conditions are

$$\begin{gathered}u_1(x, 0) = u_2(x, 0) = u_3(x, 0) = 0, \quad \eta(x, 0) = 0, \\ h_2(x, 0) = \begin{cases} h_{2_0} & \text{for} \quad x \le x_0, \\ H_0 & \text{for} \quad x > x_0, \end{cases} \\ h_3(x, 0) = \begin{cases} h_{3_0} & \text{for} \quad x \le x_0, \\ H_0 & \text{for} \quad x > x_0, \end{cases}\end{gathered} \tag{2.10}$$

where $x_0 \equiv 1$ is used in all the computations, whereas h_{2_0}, h_{3_0}, and H_0 are to be varied. The corresponding boundary conditions are

$$\begin{gathered}u_1(0, t) = u_2(0, t) = u_3(0, t) = 0, \qquad t > 0, \\ (h_2)_x\big|_{x=0} = (h_3)_x\big|_{x=0} = 0, \qquad \eta_x\big|_{x=0} = 0, \qquad t > 0, \\ h_2 \to H_0, \qquad h_3 \to H_0, \qquad \eta \to 0 \qquad \text{as} \quad x \to \infty, \quad t > 0.\end{gathered} \tag{2.11}$$

The flux conditions for h_2, h_3, and η result from symmetry considerations. To handle the case of steady injection, the boundary conditions at the wall are altered to

$$u_2(0,t) = u_{2_0}, \quad h_2(0,t) = h_{2_0}, \quad h_3(0,t) = h_{3_0}, \quad t > 0, \tag{2.12}$$

where the constant volume rate of injection per unit width is given by $u_{2_0}(h_{2_0} - h_{3_0})$.

Adopting the position that density differences among the three layers are small, we develop a "weak stratification" model by dropping terms of $O(g_1'/g)$ and $O(g_3'/g)$ from the above set of equations as well as employing the approximations

$$(g_3' - g_2')/g_1' \approx 1, \qquad g_2'/g_1' \approx 1,$$

in these equations to get

$$\frac{\partial u_2}{\partial t} + \frac{\partial}{\partial x}\left(\frac{1}{2}\,u_2^2 + h_2 + \eta\right) = 0, \tag{2.13}$$

$$\frac{\partial h_2}{\partial t} + \frac{\partial}{\partial x}\left(h_3 u_3 + (h_2 - h_3)u_2\right) = 0, \tag{2.14}$$

$$\frac{\partial u_3}{\partial t} + \frac{\partial}{\partial x}\left(\frac{1}{2}\,u_3^2 + h_2 + h_3 + \eta\right) = 0, \tag{2.15}$$

$$\frac{\partial h_3}{\partial t} + \frac{\partial}{\partial x}\left(h_3 u_3\right) = 0, \tag{2.16}$$

together with the pair of algebraic relations

$$\begin{aligned}\eta = {} & (h_{2_0} - h_{3_0})u_{2_0}^2 - (h_2 - h_3)u_2^2 - (1 - h_2)u_1^2 - h_3 u_3^2 \\ & + (h_{2_0}^2 - h_2^2)/2 + (h_{3_0}^2 - h_3^2)/2,\end{aligned} \tag{2.17}$$

$$u_1 = \frac{(h_{2_0} - h_{3_0})}{1 - h_2}\,u_{20} - \frac{(h_2 - h_3)}{1 - h_2}\,u_2 - \frac{h_3 u_3}{1 - h_2}. \tag{2.18}$$

The expression for η suggests that in the absence of injection, the free surface will experience a depression.

It should be noted that in the limit

$$h_2 \to h_3 = h, \qquad g_1' \to g_3' = g', \qquad g_2' \to 0,$$

the system (2.13)–(2.16) reduces to the weakly stratified (Boussinesq) system for the two-layer, shallow-water equations employed to study sudden releases

for bottom flows by D'Alessio et al. [10]. For that system it was found that the model equations constituted a totally hyperbolic system provided that

$$F_r^2 \equiv \left(\frac{u}{\sqrt{g'H}}\right)^2 < \left(1 - \frac{h}{H}\right)^2, \tag{2.19}$$

where u and h are the flow speed and height of the bottom current, H is the total depth of the two-layer system, and g' is the reduced gravity for the two-layer system. For that system an injection velocity of sufficient magnitude would violate the condition of (2.19). This has the effect of making the eigenvalues associated with the system complex so that the system becomes elliptic and the numerical procedure breaks down. This appears not to have been noted in the gravity current literature.

Although the model system under study in this article is too complex to allow us to obtain a simple criterion for hyperbolicity like that in (2.19), we did note a breakdown in our numerical procedure at high injection rates indicative of a switch to ellipticity of the system.

3. Numerical results

To discuss the numerical technique we begin by writing the systems (2.2)–(2.7) and (2.13)–(2.16) in the vector conservation form given by

$$\mathbf{u}_t + \mathbf{F}(\mathbf{u})_x = \mathbf{0}. \tag{3.1}$$

For the system (2.2)–(2.7) we have

$$\mathbf{u} = \begin{pmatrix} u_1 \\ \eta \\ u_2 \\ h_2 \\ u_3 \\ h_3 \end{pmatrix}, \qquad \mathbf{F}(\mathbf{u}) = \begin{pmatrix} \frac{1}{2}u_1^2 + \eta \\ [(1+\frac{g_1'}{g}\eta - h_2)u_1 + (h_2 - h_3)u_2 + h_3u_3]/(\frac{g_1'}{g}) \\ \frac{1}{2}u_2^2 + h_2 + (1-\frac{g_1'}{g})\eta \\ (h_2 - h_3)u_2 + h_3u_3 \\ \frac{1}{2}u_3^2 + \frac{g_2'}{g_1'}h_3 + (\frac{g_3'-g_2'}{g_1'})h_2 + (1-\frac{g_3'}{g})\eta \\ h_3u_3 \end{pmatrix}$$

whereas our model equations (2.13)–(2.16) can be recast in the form (3.1) with

$$\mathbf{u} = \begin{pmatrix} u_2 \\ h_2 \\ u_3 \\ h_3 \end{pmatrix}, \qquad \mathbf{F}(\mathbf{u}) = \begin{pmatrix} \frac{1}{2}u_2^2 + h_2 + \eta \\ (h_2 - h_3)u_2 + h_3u_3 \\ \frac{1}{2}u_3^2 + h_3 + h_2 + \eta \\ h_3u_3 \end{pmatrix}.$$

Numerical solutions to the above systems of conservation laws are obtained using MacCormack's method [13]. This method is an explicit conservative finite-difference scheme possessing second-order accuracy. The fact that the scheme is conservative guarantees that if convergence is achieved it will be to a physical weak solution of the hyperbolic system of equations [13]. Because of the second-order accuracy this method provides sharp resolution of shocks. Further, this scheme does not require the evaluation of the Jacobian of the flux vector and hence is easier to implement. One drawback associated with this method is the occurrence of oscillations around the shock due to numerical dispersion. These oscillations can be adequately damped by applying artificial viscosity as was first proposed by Lapidus [14].

MacCormack's method for solving the hyperbolic system (3.1) is a two-step procedure that first uses forward differencing followed by backward differencing to achieve the second-order accuracy. The scheme is given by

$$\begin{aligned} \mathbf{u}_j^* &= \mathbf{u}_j^n - \frac{\Delta t}{\Delta x}\left[\mathbf{F}(\mathbf{u}_{j+1}^n) - \mathbf{F}(\mathbf{u}_j^n)\right], \\ \mathbf{u}_j^{n+1} &= \frac{1}{2}\left(\mathbf{u}_j^n + \mathbf{u}_j^*\right) - \frac{\Delta t}{2\Delta x}\left[\mathbf{F}(\mathbf{u}_j^*) - \mathbf{F}(\mathbf{u}_{j-1}^*)\right], \end{aligned} \tag{3.2}$$

where the superscripts have been used to denote the time level while subscripts have been used to label space grid points. In all the computations performed, appropriate values for Δt and Δx are found to be $\Delta t = 0.002$ and $\Delta x = 0.01$.

To achieve convergence and to dampen oscillations around the shock, artificial viscosity is applied. This is necessary to overcome the numerical instabilities that can occur near shocks and is implemented as follows. If $\mathbf{u}_j^{n+1}$ denotes the value obtained by the scheme then the new approximation to the solution at the $n+1$ time step, $\bar{\mathbf{u}}_j^{n+1}$, is given by

$$\bar{\mathbf{u}}_j^{n+1} = \mathbf{u}_j^{n+1} + \nu \frac{\Delta t}{\Delta x} \Delta\left\{\left|\Delta \mathbf{u}_{j+1}^{n+1}\right| \Delta \mathbf{u}_{j+1}^{n+1}\right\}, \tag{3.3}$$

where ν is an adjustable parameter known as the artificial viscosity and Δ refers to a backward difference operator. Thus the expression

$$\nu \frac{\Delta t}{\Delta x} \Delta\{|\Delta \mathbf{u}| \Delta \mathbf{u}\}$$

attempts to approximate the diffusion term

$$\nu \frac{\Delta t}{\Delta x} (\Delta x)^3 (|\mathbf{u}_x| \mathbf{u}_x)_x.$$

Adding this quantity has a smoothing effect on the numerical results and, being of third order, does not alter the truncation error of the difference

scheme. Although we do not carry out a lengthy investigation into the optimal value of ν we find that $\nu = 1$ is sufficient in all our computations.

The first objective of our numerical calculations is to demonstrate that our model equations (2.13)–(2.16) capture the essential dynamics of the flow field governed by the larger system (2.2)–(2.7). We do this principally to have confidence in our later analytical work that is based upon these simpler model equations. The ability of these model equations to represent essential features of the flow is demonstrated by comparing two sets of numerical output obtained from both the model equations and the larger system. These comparisons are illustrated in Figures 2A and 2B. Portrayed in Figure 2A is the gravity current predicted by both sets of equations for the case with no injection. In this figure, as well as all others to be presented, the initial configuration is given by the dashed line. The density differences are taken to be $\rho_2 - \rho_1 = 0.1\rho_1$ and $\rho_3 - \rho_2 = 0.1\rho_1$ with the plot corresponding to a time $t = 3$. Figure 2A demonstrates that solutions for the sudden release of a fixed volume based on either the model equations or the larger system with the specified density differences are in excellent qualitative, as well as quantitative, agreement. The model equations capture the dynamics involved in rear shock formation as well as providing good agreement for the front speed. Although not depicted in this figure our numerical results indicate improved agreement as the density differences are decreased.

The model equations unlike the system (2.2)–(2.7) fail to provide information about surface gravity wave phenomena. This is to be expected since these model equations are derived under the constraint that all terms of $O(g_n'/g)$, $n = 1, 2, 3$, be neglected, which is equivalent to having the surface gravity waves propagating with infinite speed and therefore filtered out of the solutions.

As a further comparison between results based upon the model equations and those from the larger system we present, in Figure 2B, plots of gravity currents for various density differences at $t = 10$. The ability of the model equations to provide reasonable agreement with the larger system over a range of density differences is clearly demonstrated.

Another objective of this section is to draw certain conclusions regarding the behavior, structure, and dependence of the gravity current on the initial conditions. For the case with no injection the initial conditions involve the three arbitrary parameters h_{2_0}, h_{3_0}, and H_0. In addition to these we have two more degrees of freedom brought about by the density differences $\rho_2 - \rho_1$ and $\rho_3 - \rho_2$. The problem with injection introduces yet another parameter, namely u_{2_0}. We propose to proceed by varying these parameters in the following systematic order.

First, we focus on the case with no injection and will qualitatively address the case with injection at the end of this section. Second, numerical experimentation has shown that rather than varying the three parameters

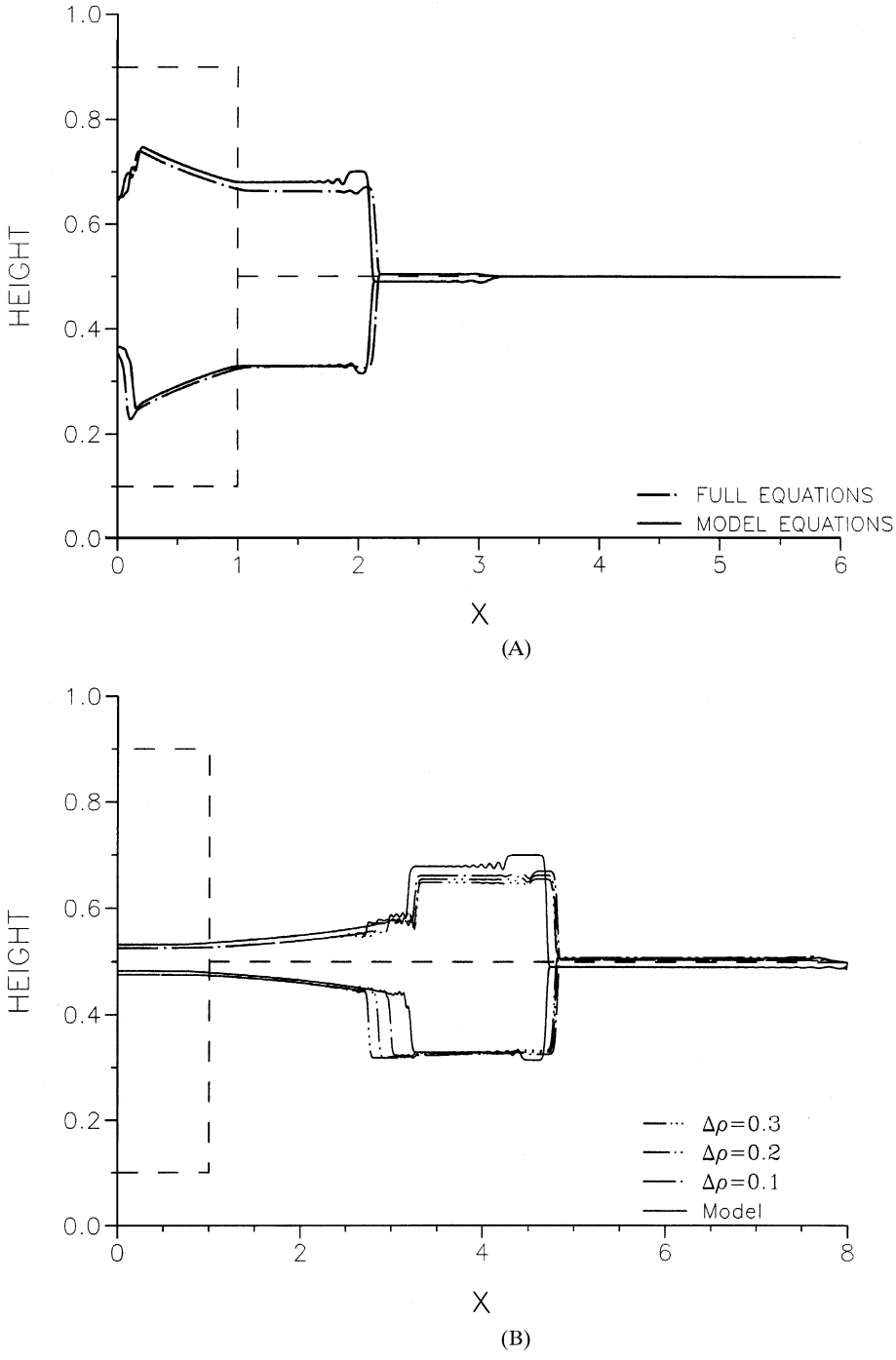

Figure 2. Comparison between model equations and 6×6 system for the intrusive gravity current (A) having $\rho_2 - \rho_1 = \rho_3 - \rho_2 = 0.1\rho_1$, $h_{2_0} = 0.9$, $h_{3_0} = 0.1$ at $t = 3$, and (B) with different density differences for the case $h_{2_0} - H_0 = H_0 - h_{3_0} = 0.4$ at $t = 10$.

h_{2_0}, h_{3_0}, H_0 independently it is more instructive to consider varying the two quantities, $h_{2_0} - H_0$ and $H_0 - h_{3_0}$, as this is a source of asymmetry in the initial profile. Another source of asymmetry is in the density differences $\rho_2 - \rho_1$ and $\rho_3 - \rho_2$. Thus, we separately consider cases where $h_{2_0} - H_0 = H_0 - h_{3_0}$ but $\rho_2 - \rho_1 \neq \rho_3 - \rho_2$ and vice versa. Doing so illustrates the consequences of the different asymmetries inherent in the problem. For convenience we set $H_0 = 0.5$ in all the plots to be presented.

In Figures 3A and 3B we show gravity currents for the case $h_{2_0} - H_0 = H_0 - h_{3_0} = 0.4$. In Figure 3A $\rho_2 - \rho_1 = 0.05\rho_1$ while $\rho_3 - \rho_2 = 0.25\rho_1$ and $t = 10$. Because of the large variation in these differences the gravity current flows almost entirely in the top layer with the bottom layer acting more or less as a solid boundary. Figure 3B, which is at a later time $t = 20$, illustrates the opposite scenario in which the gravity current flows essentially in the bottom layer owing to the choices $\rho_2 - \rho_1 = 0.15\rho_1$ and $\rho_3 - \rho_2 = 0.05\rho_1$. In both Figures 3A and 3B, it is seen that the intermediate layer quickly slumps from any isostatically uncompensated state to its Archimedean level with $(h_2 - H_0)(\rho_2 - \rho_1) = (H_0 - h_3)(\rho_3 - \rho_2)$ and hence the corresponding vertical motion creates a wave of the opposite sign ahead of the intrusion on the interface between the upper and lower layers. It should be noted that the solutions in Figures 3A and 3B are obtained using the larger system rather than the model equations owing to the large density differences employed there.

Displayed in Figures 4A and 4B are gravity currents corresponding to $\rho_2 - \rho_1 = \rho_3 - \rho_2 = 0.1\rho_1$. In Figure 4A $h_{2_0} - H_0 = 0.4$, $H_0 - h_{3_0} = 0$, and $t = 10$. Once again we observe a large disturbance propagating along the interface separating the top and bottom layers. The structure of the gravity current is more complicated than in previous cases and without symmetry about the height $H_0 = 0.5$. Figure 4B illustrates the opposite case where $h_{2_0} - H_0 = 0$, $H_0 - h_{3_0} = 0.4$, and $t = 10$. As expected, the disturbance along the interface is inverted with respect to the case shown in Figure 4A. Such interface disturbances have been observed in experiments reported on by Simpson [1].

Shown in Figure 5 is the time evolution of a gravity current as predicted by the model equations with $h_{2_0} - H_0 = H_0 - h_{3_0} = 0.4$. Since we have symmetry in both the initial profile and density differences we expect a symmetric gravity current to result as observed. Here the gravity current possesses a well-defined head with a rear shock that travels faster than the front and overtakes it at $t \simeq 31$. At this time the gravity current assumes a self-similar structure.

In Figure 6 is shown a situation in which no rear shock has formed. Here the release volume occupies a 50%, symmetrically located, portion of the total fluid depth. In Figure 7 is depicted a situation in which a rear shock forms in the upper part of the flow but not the bottom part.

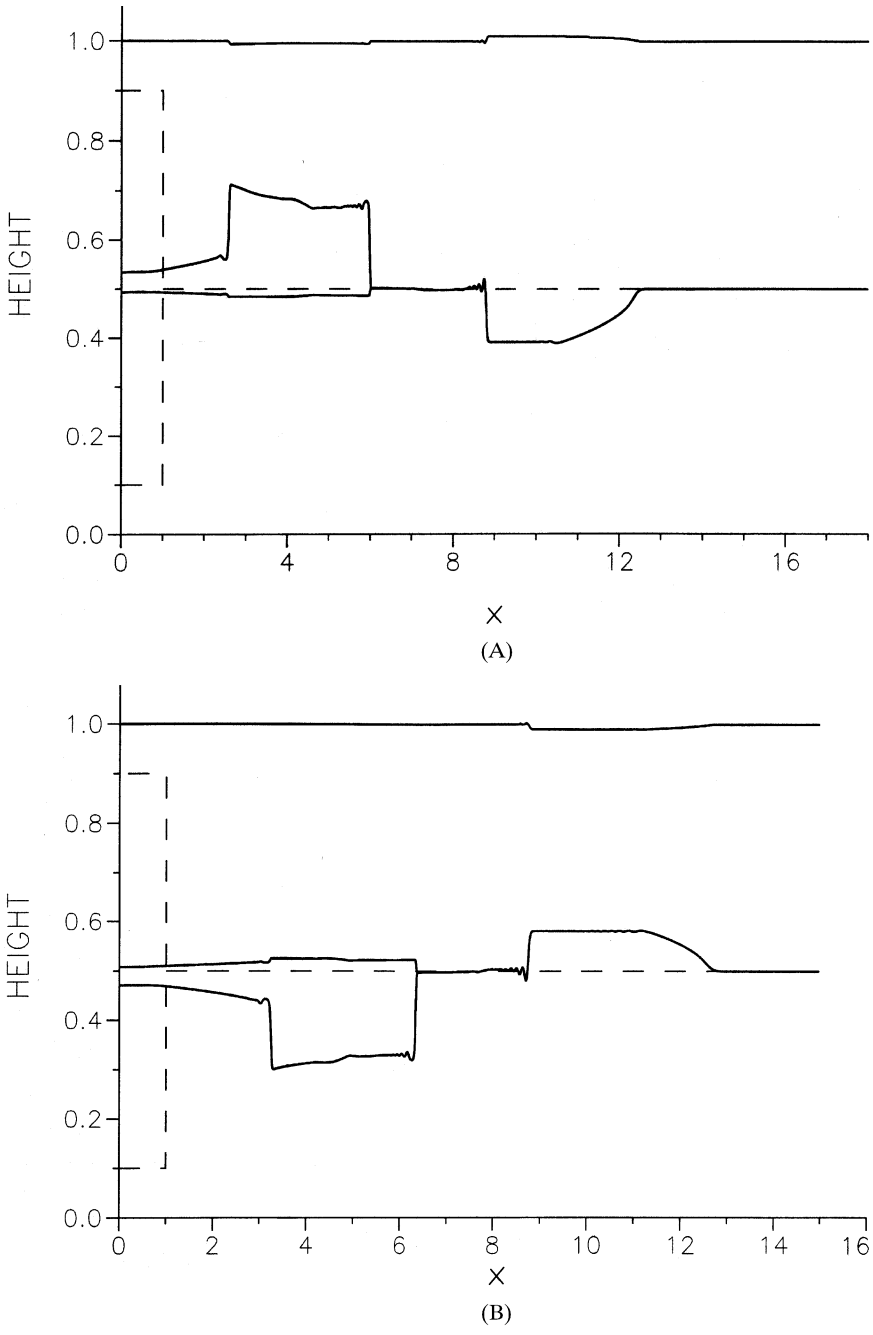

Figure 3. The gravity current and free surface for the case (A) $\rho_3 - \rho_2 \gg \rho_2 - \rho_1$ and $h_{2_0} - H_0 = H_0 - h_{3_0} = 0.4$ at $t = 10$, and (B) $\rho_2 - \rho_1 \gg \rho_3 - \rho_2$ and $h_{2_0} - H_0 = H_0 - h_{3_0} = 0.4$ at $t = 20$.

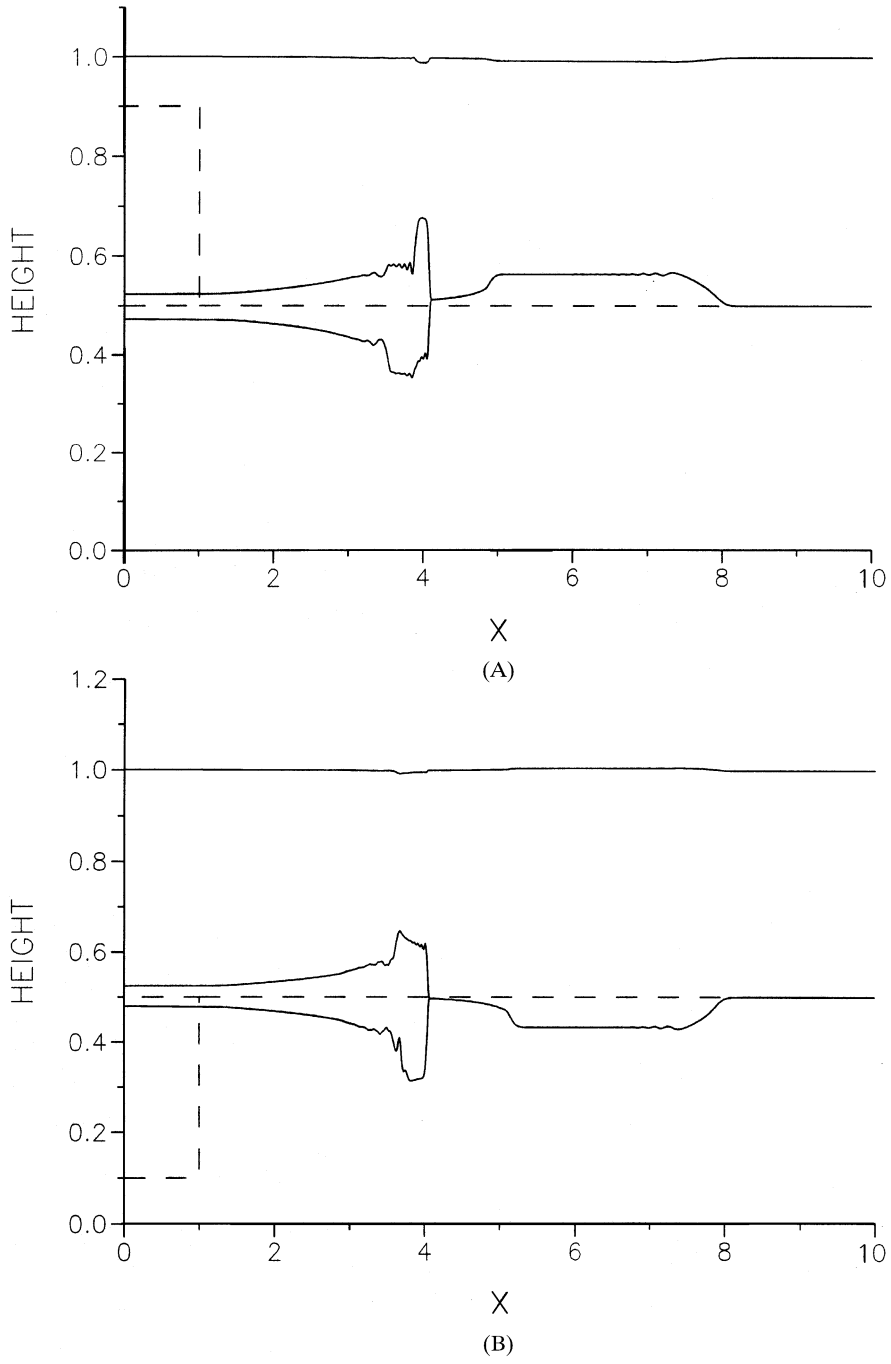

Figure 4. The gravity current and free surface for the case (A) $h_{2_0} - H_0 = 0.4$, $H_0 - h_{3_0} = 0$ and $\rho_3 - \rho_2 = \rho_2 - \rho_1 = 0.1\rho_1$ at $t = 10$, and (B) $h_{2_0} - H_0 = 0$, $H_0 - h_{3_0} = 0.4$ and $\rho_3 - \rho_2 = \rho_2 - \rho_1 = 0.1\rho_1$ at $t = 10$.

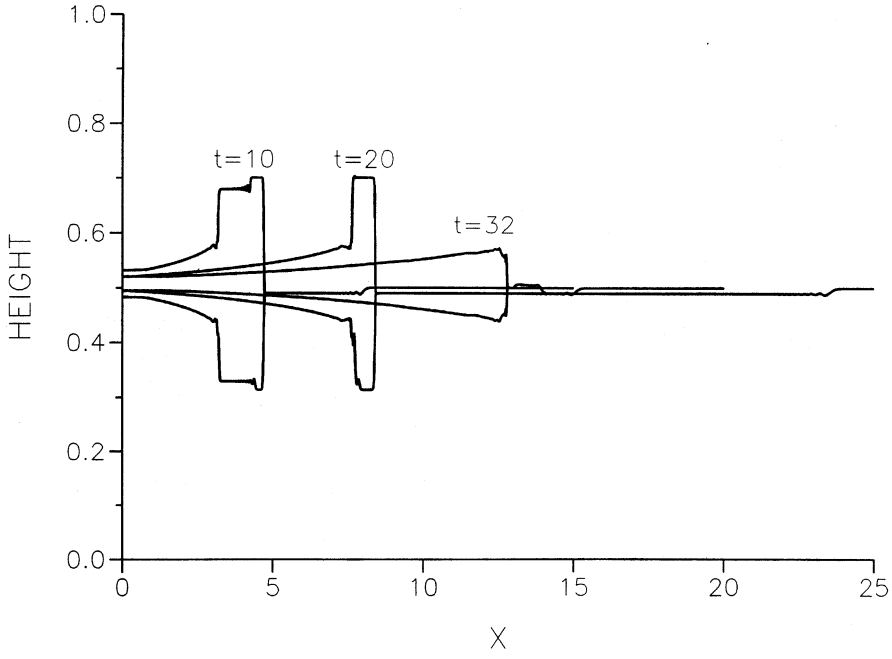

Figure 5. The time evolution of the gravity current with $h_{2_0} - H_0 = H_0 - h_{3_0} = 0.4$ and $\rho_3 - \rho_2 = \rho_2 - \rho_1$.

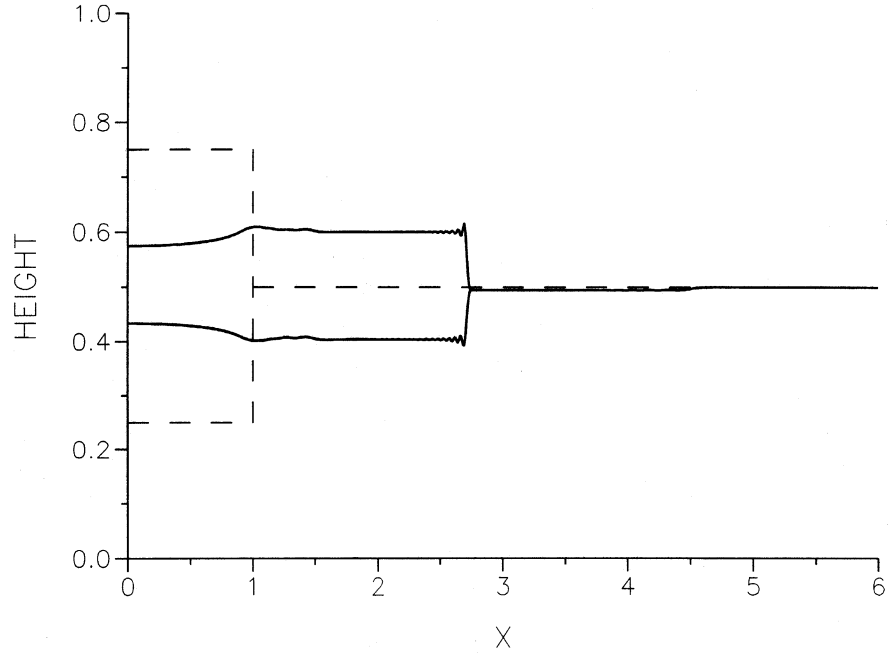

Figure 6. A plot of a gravity current possessing no rear shocks having $h_{2_0} - H_0 = H_0 - h_{3_0} = 0.25$ and $\rho_3 - \rho_2 = \rho_2 - \rho_1$ at $t = 5$.

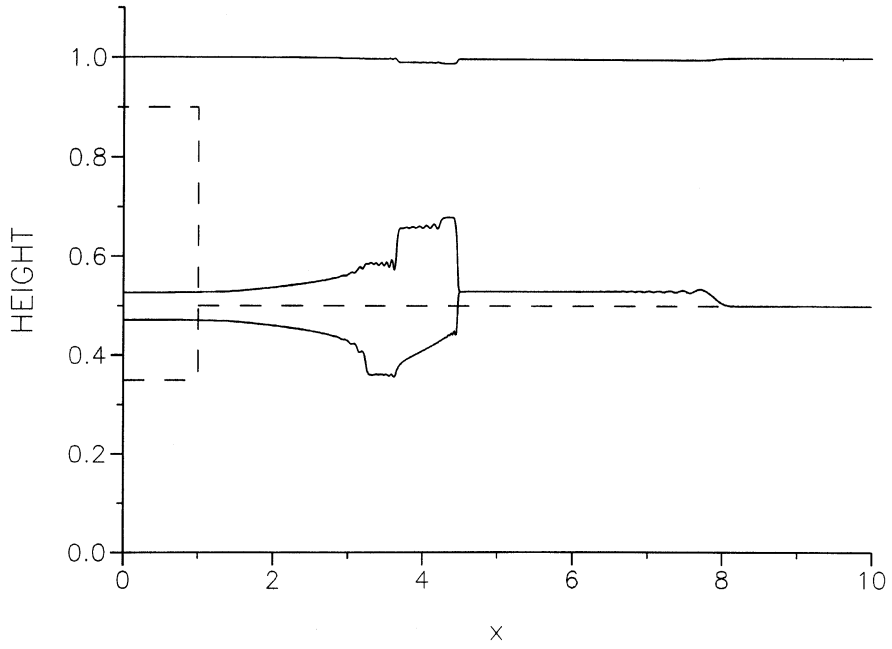

Figure 7. A plot of a gravity current possessing a rear shock in the top half while no shock in the bottom half with $h_{2_0} - H_0 = 0.4$, $H_0 - h_{3_0} = 0.15$ and $\rho_3 - \rho_2 = \rho_2 - \rho_1$ at $t = 10$.

From the numerical work presented so far we may speculate that the formation of a rear shock in the gravity flow is related to the velocity developed in the associated backflow. Contrasting the results shown in Figures 5 and 6 we know, from the condition of no net volume flux in the absence of injection, that the backflow in Figure 5 will be of higher velocity than that for the scenario depicted in Figure 6. It is the interaction of the backflow with the endwall that produces the rear shock and to do so this backflow must be of sufficient vigor. This reasoning may also be applied to the result shown in Figure 7.

In Figure 8 we have included some numerical results to indicate the degree to which our model equations reproduce the results obtained using the system (2.2)–(2.7) for the case of injection. In this figure we have $h_{2_0} - H_0 = H_0 - h_{3_0} = 0.25$, $\rho_2 - \rho_1 = \rho_3 - \rho_2 = 0.1\rho_1$, and $u_{2_0} = 0.1$ with $t = 3$. From the results shown here it would appear that the model equations capture the essential dynamics in the steady injection case.

Some analytical results in the form of similarity solutions may be obtained for the case of a thin gravity current. Since the current is thin ($h_2 - h_3 \ll 1$) it has little effect on the free surface so that we make the approximation $\eta \approx 0$ and decouple the equations governing the flow of the intrusion from those

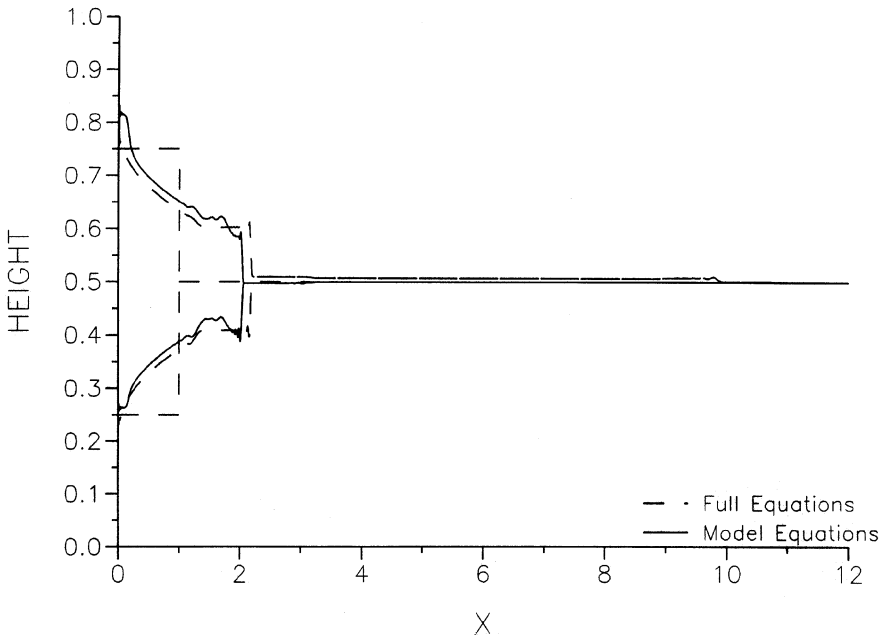

Figure 8. Comparison between model equations and 6×6 system for the intrusive gravity current for the case of steady injection with $h_{2_0} = 0.75$, $h_{3_0} = 0.25$, $u_{2_0} = 0.1$, and $\rho_2 - \rho_1 = \rho_3 - \rho_2 = 0.1\rho_1$ at $t = 3$.

for the ambient fluids. Equations (2.4) and (2.5) then become

$$\frac{\partial u}{\partial t} + \frac{\partial}{\partial x}\left[\frac{1}{2}u^2 + \overline{h}_2\right] = 0, \tag{3.4}$$

$$\frac{\partial}{\partial t}(\overline{h}_2 + \overline{h}_3) + \frac{\partial}{\partial x}[(\overline{h}_2 + \overline{h}_3)u] = 0, \tag{3.5}$$

where $u(x, t)$ $(\equiv u_2)$ is the velocity in the gravity current, and $\overline{h}_2$ and $\overline{h}_3$ represent the depth of the gravity current above and below the interface between the upper and lower fluids, respectively (i.e., $\overline{h}_2 \equiv h_2 - H_0$, $\overline{h}_3 \equiv H_0 - h_3$).

Similarity solutions to Equations (3.4) and (3.5) can be obtained if, together with the boundary conditions at $x = 0$, we apply the Rankine–Hugoniot jump conditions to the discontinuity at the moving front of the gravity current.

In the case of steady injection, the similarity transformation

$$\overline{h}_2(x, t) = f(\xi), \qquad \overline{h}_3(x, t) = g(\xi), \qquad u(x, t) = v(\xi), \tag{3.6}$$

where

$$\xi = x/t \tag{3.7}$$

reduces Equations (3.4) and (3.5) to the pair of ordinary differential equations

$$f' + (v - \xi)v' = 0, \qquad (v - \xi)(f' + g') + (f + g)v' = 0. \tag{3.8}$$

The solution to these equations corresponding to a physically realistic flow is

$$\begin{aligned} v(\xi) &= u_0, & 0 < \xi < \xi_1, \\ f(\xi) &= h_{2_0} - H_0, & 0 < \xi < \xi_1, \\ g(\xi) &= H_0 - h_{3_0}, & 0 < \xi < \xi_1, \end{aligned} \tag{3.9}$$

where $\xi_1 = u_0$ and u_0 satisfies

$$u_0^2 = 2(h_{2_0} - H_0). \tag{3.10}$$

This indicates that in the case when the intermediate fluid is injected at a constant rate the gravity current, in the self-similar stage, is of uniform thickness along its entire length advancing with the velocity at which it is being injected. This is in agreement with what is predicted by the numerical solution of the shallow-water equations as can be seen from Figure 9.

For the sudden release of a fixed volume similarity solutions of the governing equations can be obtained for two particular cases related to the differences between the densities of the fluids. In the first case the density of the gravity current is the mean of the densities of the upper and lower fluids. In this instance the gravity current will ultimately be symmetric with respect to the interface between the upper and lower fluids. The other case for which we can obtain a similarity solution arises when the density of the gravity current is much closer in value to that of one of the surrounding fluids than the other. For example, if $\rho_3 - \rho_2 \gg \rho_2 - \rho_1$ the gravity current will eventually flow above the lower fluid regardless of where it was released. In both cases, Equations (3.4) and (3.5) can be written in terms of the thickness of the gravity current $\overline{h}$ to give

$$\frac{\partial u}{\partial t} + \frac{\partial}{\partial x}\left[\frac{1}{2}u^2 + \overline{h}\right] = 0, \tag{3.11}$$

$$\frac{\partial \overline{h}}{\partial t} + \frac{\partial}{\partial x}(\overline{h}u) = 0. \tag{3.12}$$

The similarity transformation [7, 15]

$$\overline{h}(x, t) = t^{-2/3} f(\xi), \qquad u(x, t) = t^{-1/3} v(\xi), \qquad \xi = t^{-2/3} x, \tag{3.13}$$

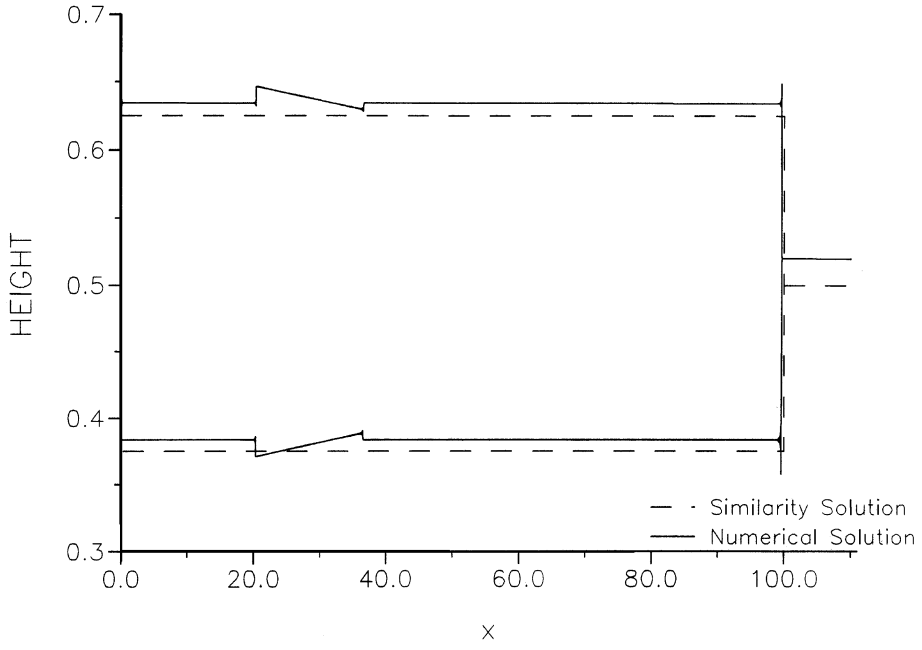

Figure 9. Comparison between the similarity solution and the numerical solution for the injection case; $t = 200$, $h_{2_0} = 0.625$, $h_{3_0} = 0.375$, and $u_0 = 0.5$.

satisfies the fixed volume constraint and reduces (3.11), (3.12) to the pair of coupled nonlinear equations

$$f' - \frac{1}{3}\, v + \left(v - \frac{2}{3}\, \xi\right) v' = 0, \qquad -\frac{2}{3}(\xi f)' + (fv)' = 0. \tag{3.14}$$

These equations can be solved to yield

$$\begin{aligned} v(\xi) &= \frac{2}{3}\, \xi, & 0 < \xi < \xi_1, \\ f(\xi) &= \frac{1}{9}(\xi^2 + \xi_1^2), & 0 < \xi < \xi_1, \end{aligned} \tag{3.15}$$

with

$$\xi_1 = \frac{3}{2}\left[(h_{2_0} - h_{3_0})x_0\right]^{1/3}. \tag{3.16}$$

Comparisons between the similarity solutions and results obtained from numerical integrations of the shallow-water equations are presented in Figures 10 and 11. These results serve as a check on the numerical scheme.

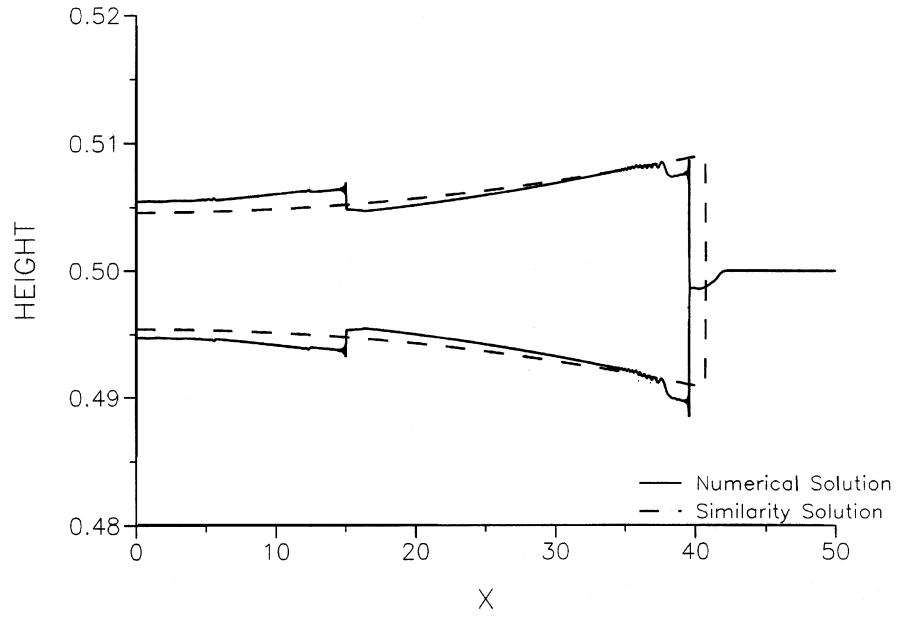

Figure 10. Comparison between the similarity solution and the numerical solution for a symmetric gravity current resulting from a sudden release of a fixed volume of fluid; $t = 200$, $h_{2_0} = 0.6$, $h_{3_0} = 0.1$, $x_0 = 1$, and $H_0 = 0.5$.

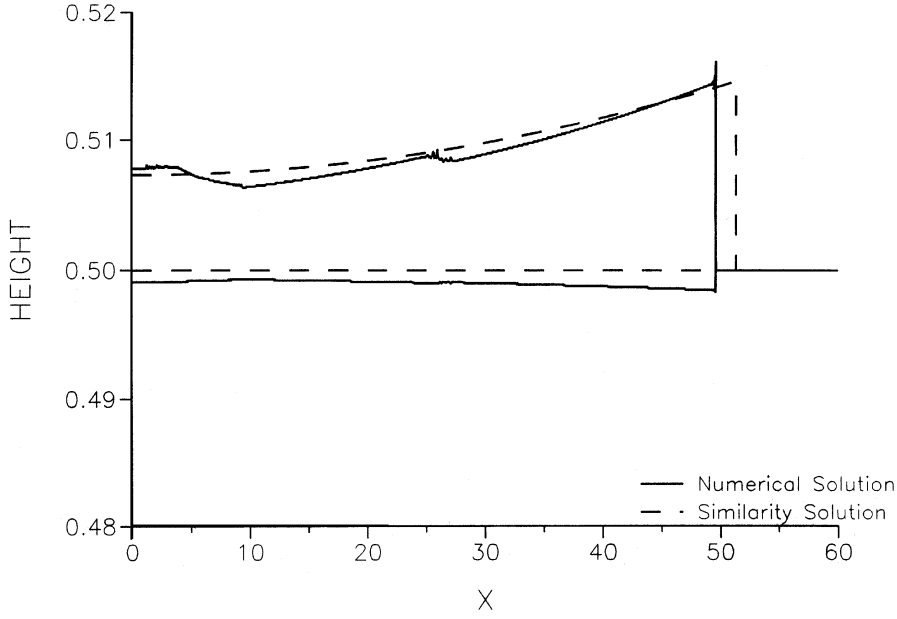

Figure 11. Comparison between the similarity solution and the numerical solution for the sudden release of a fixed volume of fluid problem for the case when $\rho_3 - \rho_2 \gg \rho_2 - \rho_1$; $t = 200$, $h_{2_0} = 0.6$, $h_{3_0} = 0.1$, $x_0 = 1$. The numerical solution was obtained with $\rho_2 = 1.04\rho_1$ and $\rho_3 = 1.4\rho_1$.

4. Bore formation and wavefront expansions

We now employ wavefront expansions [16] in conjunction with our weak stratification model to study internal bore formation associated with intrusive gravity flows. This method enables us to compute the growth rate for a first derivative discontinuity across the wavefront, thereby obtaining the breaking time, t_B, for a wave traveling on the interface between two different fluids. This method involves a formal expansion procedure that provides the same information that can be obtained by taking limits in the differential equations as is done in acceleration wave analysis [17].

Our weak stratification model when written as a first-order system is

$$\frac{\partial \mathbf{u}}{\partial t} + \mathbf{a}(\mathbf{u})\,\frac{\partial \mathbf{u}}{\partial x} = \mathbf{0}, \tag{4.1}$$

where

$$\mathbf{u} = (u_2, h_2, u_3, h_3)^T, \tag{4.2}$$

and

$$\mathbf{a} = \begin{pmatrix} \left(u_2 + \frac{\partial \eta}{\partial u_2}\right) & \left(1 + \frac{\partial \eta}{\partial h_2}\right) & \frac{\partial \eta}{\partial u_3} & \frac{\partial \eta}{\partial h_3} \\ (h_2 - h_3) & u_2 & h_3 & (u_3 - u_2) \\ \frac{\partial \eta}{\partial u_2} & \left(1 + \frac{\partial \eta}{\partial h_2}\right) & \left(u_3 + \frac{\partial \eta}{\partial u_3}\right) & 1 + \frac{\partial \eta}{\partial h_3} \\ 0 & 0 & h_3 & u_3 \end{pmatrix}, \tag{4.3}$$

with η given by (2.17).

If the first derivatives are discontinuous we expand the state variables in the form

$$\begin{aligned} u_j &= u_j^{(0)}, && \xi > 0, \\ u_j &= u_j^{(0)} + u_j^{(1)}(t)\xi + \tfrac{1}{2}\, u_j^{(2)}(t)\xi^2 + \ldots, && \xi < 0, \end{aligned} \tag{4.4}$$

where $\xi = x - X(t)$ so that $\xi = 0$ corresponds to the wavefront. In (4.4) $\mathbf{u}^{(0)}$ refers to the constant state ahead of the lead characteristic, that is,

$$\mathbf{u}^{(0)} = (u_j^{(0)}) = \begin{pmatrix} 0 \\ h_{2_0} \\ 0 \\ h_{3_0} \end{pmatrix}. \tag{4.5}$$

The coefficients in (4.4) are determined by inserting these expansions into (4.1) and equating terms. This leads to the hierarchy of equations

$$a_{ij}^{(0)} u_j^{(1)} - c u_i^{(1)} = 0, \tag{4.6}$$

$$a_{ij}^{(0)} u_j^{(2)} - c u_i^{(2)} + \left\{ \frac{du_i^{(1)}}{dt} + \frac{\partial a_{ij}^{(0)}}{\partial u_k} u_j^{(1)} u_k^{(1)} \right\} = 0, \tag{4.7}$$

and so on, where c denotes $\dot{X}(t)$ and the superscript zero means that the argument of the corresponding function is $\mathbf{u}^{(0)}$. Equation (4.6) gives for the values of c

$$c = \pm c_{\pm}, \tag{4.8}$$

where

$$\begin{aligned} c_{\pm} = \{ & \tfrac{1}{2} [h_{3_0}(1 - h_{3_0}) + h_{2_0}(1 - h_{2_0})] \\ & \pm \left[\left(\tfrac{1}{2} [h_{3_0}(1 - h_{3_0}) + h_{2_0}(1 - h_{2_0})] \right)^2 \right. \\ & \left. - h_{3_0}(1 - h_{2_0})(h_{2_0} - h_{3_0}) \right]^{1/2} \}^{1/2}. \end{aligned} \tag{4.9}$$

Since (4.1) is totally hyperbolic and $\mathbf{a}^{(0)}$ has a null space of dimension one we may write [18]

$$u_j^{(1)} = \sigma L_j, \tag{4.10}$$

where $\mathbf{L}$ is a right eigenvector of $a_{ij}^{(0)}$ corresponding to the eigenvalue c. Applying the corresponding left eigenvector $\boldsymbol{\ell}$ to (4.7), inserting $u_j^{(1)}$ from (4.10) and using the fact that for hyperbolic systems $\ell_i L_i \neq 0$ we arrive at a nonlinear evolution equation for the coefficient σ, that is,

$$\frac{d\sigma}{dt} + \ell_i \frac{\partial a_{ij}^{(0)}}{\partial u_k} L_j L_k \sigma^2 / \ell_n L_n = 0. \tag{4.11}$$

The nonvanishing of the coefficient of σ^2 in (4.11) is closely related to the genuine nonlinearity of the characteristic field [19].

Integrating in (4.11) gives

$$\sigma(t) = \frac{\sigma(0)}{1 + q_0 \sigma(0) t}, \tag{4.12}$$

where

$$q_0 \equiv \left[\ell_i \frac{\partial a_{ij}}{\partial u_k} L_j L_k / \ell_n L_n \right]_{\mathbf{u}=\mathbf{u}^{(0)}}. \tag{4.13}$$

As we are specifically interested in the possibility of infinite slopes (shocks) developing in finite time at the interfaces between the fluids of different densities we examine those coefficients of (4.4) that represent the values of

the spatial derivatives of the interface height. These are $u_2^{(1)} \equiv h_2^{(1)}(t)$ and $u_4^{(1)} \equiv h_3^{(1)}(t)$, which are given in terms of their initial values by

$$h_2^{(1)}(t) = \frac{h_2^{(1)}(0)A}{A + q_0 h_2^{(1)}(0)t}, \tag{4.14}$$

$$h_3^{(1)}(t) = \frac{h_3^{(1)}(0)}{1 + q_0 h_3^{(1)}(0)t}, \tag{4.15}$$

where

$$A \equiv \frac{c^2 - h_{3_0}(1 - h_{3_0})}{h_{3_0}(1 - h_{2_0})}\,. \tag{4.16}$$

We now choose initial conditions corresponding to a deflection of the otherwise uniform upper surface of the intermediate layer. These we take as

$$\begin{gathered} h_2(x,t)\big|_{t=0} = h_{2_0} + f(x), \\ h_3 = h_{3_0}, \qquad u_2 = u_3 = 0, \qquad t = 0, \end{gathered} \tag{4.17}$$

where $f(x)$ is compactly supported on $0 < x < x_1$ with $f'(x_1) \neq 0$. Then, since the lead characteristic for waves traveling to the right is given by

$$x = c_+ t + x_1, \tag{4.18}$$

the time for shock initiation is obtained by equating the denominator in (4.14) to zero ($h_2^{(1)}(t) \to \infty$) to get a breaking time t_{B}, where

$$t_{\mathrm{B}} = \frac{-A^+}{q_0^+ f'(x_1)}, \tag{4.19}$$

with A^+ and q_0^+ having the meaning that where an eigenvalue appears in either of A or q_0 it is taken to be the particular eigenvalue c_+ defined in (4.9). It is of interest to note here that $q_0^+ \to 0$ (and hence $t_{\mathrm{B}} \to \infty$) corresponds to a local linear degeneracy at the wavefront [20]. A lengthy calculation gives for q_0^+ that

$$\begin{aligned} q_0^+ = \Bigg(& -1 + \frac{1}{H_0} + \frac{c_+^2}{h_{3_0} H_0} - \frac{(c_+^2 - h_{3_0} H_3)^2}{h_{3_0}^2 H_2^2} - \frac{(c_+^2 - H_0 H_2)}{h_0 H_2} \\ & + \frac{2(c_+^2 H_3 - H_0 H_2)}{h_{3_0} H_0 H_2} - \frac{(c_+^2 - H_0 H_2)(c_+^2 - h_{3_0} H_3)^2}{h_{3_0}^2 H_0 H_2^3} \\ & + \frac{(c_+^2 - h_{3_0})(c_+^2 - h_{3_0} H_3)}{h_{3_0}^2 H_0 H_2} + \frac{(c_+^2 - h_{3_0})}{h_{3_0}^2 H_0 H_2} \left(c_+^2 - h_{3_0}(H_2 + H_3)\right) \end{aligned}$$

$$+\frac{(c_+^2-h_{3_0})}{c_+h_{3_0}}\left[\left(\frac{c_+^2-h_{3_0}}{c_+h_{3_0}}\right)\left(1-\frac{2H_0H_3}{H_2}\right)-\frac{2c_+H_0}{H_2}\right]$$
$$-\frac{2c_+}{h_{3_0}H_2}\left[\frac{(c^2-h_{3_0})H_0}{c_+}+c_+(1-H_0)\right]$$
$$-\frac{2(c_+^2-H_0H_2)(c_+^2-h_{3_0})}{c_+h_{3_0}H_2^2}\left(c_++\frac{(c_+^2-h_{3_0})H_3}{c_+h_{3_0}}\right)+\frac{c_+(c_+^2-H_0H_2)}{h_{3_0}^2H_0H_2^2}$$
$$\times\left[-\frac{2h_{3_0}H_0}{c_+}(c_+^2-h_{3_0})+c_+(H_2-2h_{3_0}(1-H_0))\right]\Bigg)$$
$$\times\left\{\frac{2[(h_{3_0}H_3+h_{2_0}H_2)c_+^2-2h_{3_0}H_0H_2]}{c_+h_{3_0}H_0H_2}\right\}^{-1}, \tag{4.20}$$

where $H_0 = h_{2_0} - h_{3_0}$, $H_2 = 1 - h_{2_0}$, and $H_3 = 1 - h_{3_0}$.

The wavefront expansion technique predicts that the breaking time, t_B, of a Lipschitz continuous initial disturbance on the interface between the upper and intermediate fluids is given by (4.19). This theoretical breaking time is plotted in Figure 12 as a function of h_{2_0} for several values of h_{3_0} with $h_2^{(1)}(0) = -1$.

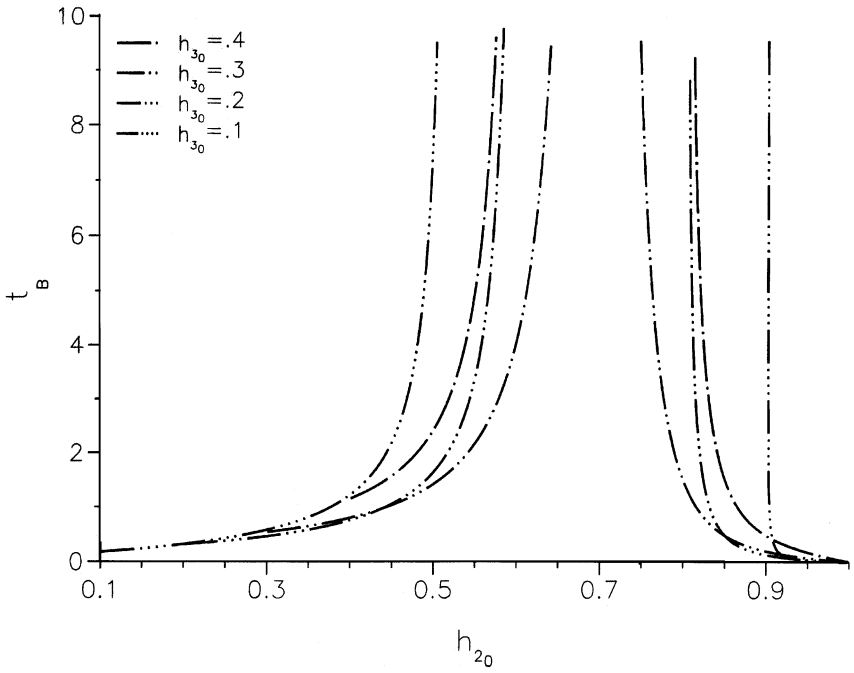

Figure 12. Plots of breaking time versus h_{2_0} for values of $h_{3_0} = 0.1, 0.2, 0.3, 0.4$.

Although the wavefront analysis is limited to the special form of wave treated here it is extremely valuable because it is always possible to carry out this calculation explicitly. A smooth profile does not have to behave in precisely the same way, but one can get a rough estimate of the magnitude of the derivatives required to produce a breaking wave and an estimate of the time of breaking [16]. For our problem, since there is no dissipation, any negative initial derivative at the front will produce a shock at the front provided the characteristic field is not degenerate there. The smaller the amplitude of this derivative the longer it takes to form a breaking wave.

It can be seen from Figure 12 that the $h_{3_0} = 0.1$ curve has vertical asymptotes, corresponding to $t_B \to \infty$, at $h_{2_0} \approx 0.5$ and $h_{2_0} \approx 0.9$ with no positive breaking time for $0.5 \lesssim h_{2_0} \lesssim 0.9$. This calculation therefore tells us that with the height of the lower layer fixed at $h_{3_0} = 0.1$ the breaking time for a front shock on the interface between the upper and intermediate layers increases as we increase the height of the intermediate layer in the range 0.1 and 0.5 becoming infinite at the upper end of this range. Then, for the range $0.5 \lesssim h_{2_0} \lesssim 0.9$ no shock forms at the leading edge. This is not to say that a shock cannot form at some other location but it will not be detected by this method. When $h_{2_0} \gtrsim 0.9$ a front shock forms in a very short time from flow initiation.

The $h_{3_0} = 0.2$ curve has vertical asymptotes at $h_{2_0} \approx 0.55$ and $h_{2_0} \approx 0.8$ so that there will be no shock formed at the lead characteristic for h_{2_0} in the range $0.55 \lesssim h_{2_0} \lesssim 0.8$ when $h_{3_0} = 0.2$. The $h_{3_0} = 0.3$ curve has a single vertical asymptote at $h_{2_0} \approx 0.7$ whereas the $h_{3_0} = 0.4$ curve has vertical asymptotes at $h_{2_0} \approx 0.55$ and $h_{2_0} \approx 0.8$.

The values of h_{2_0} between the vertical asymptotes correspond to those values of h_{2_0} for the chosen h_{3_0} such that the calculated breaking times are negative indicating that shocks do not form (at the wavefront). The values of h_{2_0} at the vertical asymptote correspond to $q_0^+ = 0$ and hence represent a local linear degeneracy at the wavefront with a breaking time $t_B \to \infty$ [20].

Figures 13 and 14 contain results obtained by numerically solving the model equations and these illustrate the time evolution of an initial disturbance on the interface between the upper and intermediate fluids. The disturbance is a single pulse of amplitude 0.1 and slope -1 at the leading edge. The disturbance is shown at the initial instant ($t = 0$) and at $t = 2$. Figure 13 corresponds to the case $h_{3_0} = 0.1$ and $h_{2_0} = 0.3$. It can be seen that by $t = 2$ the leading edge of the disturbance has steepened considerably indicating wave breaking and bore formation. Furthermore, numerical oscillations have appeared indicating the presence of a discontinuity in the solution. Thus we may conclude that our numerical results agree with the theoretical prediction based upon the wavefront analysis.

Figure 14 corresponds to the case $h_{3_0} = 0.5$ and $h_{2_0} = 0.7$. We observe that the slope at the leading edge of the disturbance has decreased in magnitude

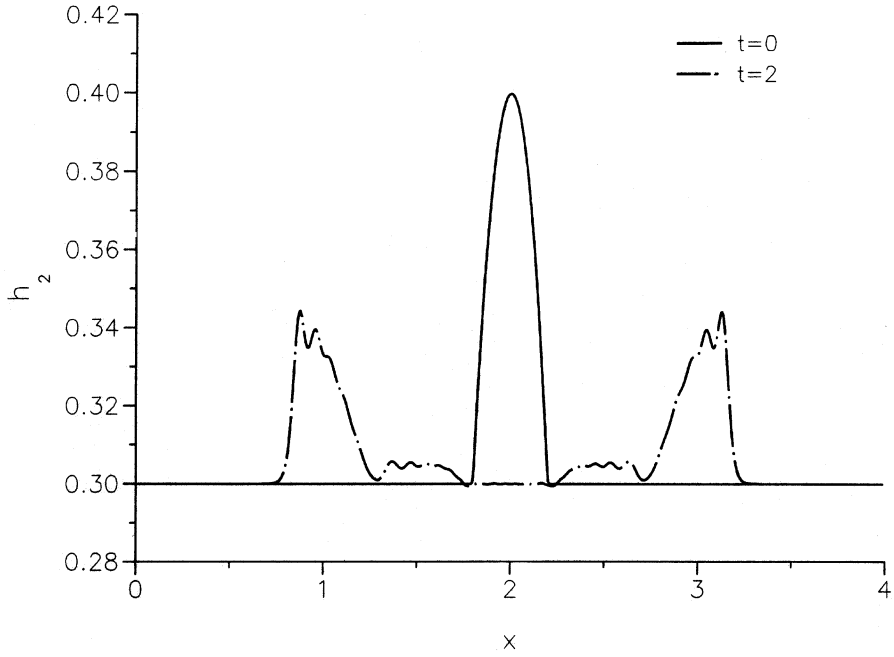

Figure 13. Evolution of an initial pulse indicating frontal bore formation.

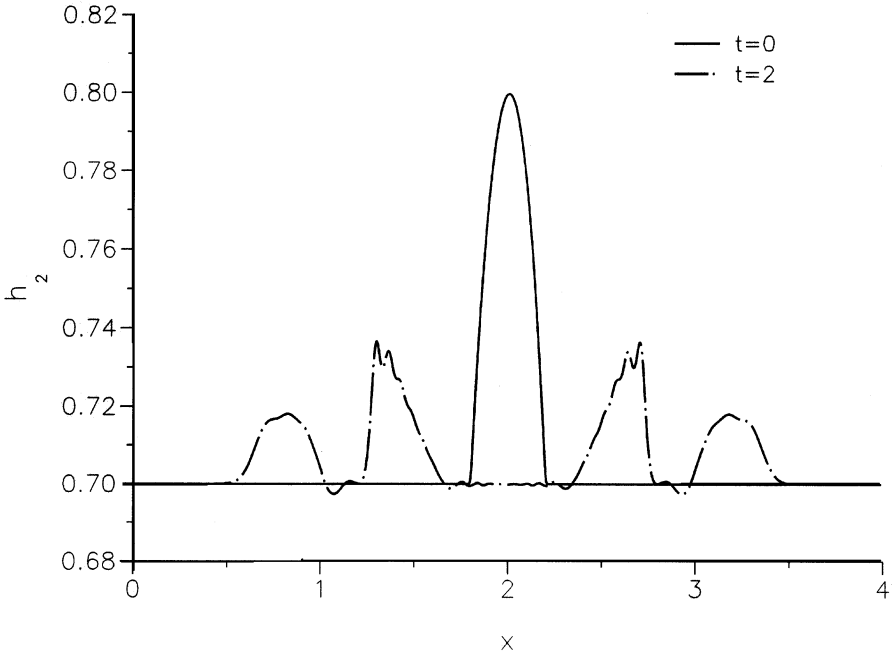

Figure 14. Evolution of an initial pulse indicating no frontal breaking.

when compared to that of the initial profile. This trend was found to persist when larger time values were considered. We may thus conclude that the numerical results predict no wave breaking at the leading edge of a right-traveling disturbance in this particular parameter regime. This agrees with the theoretical values for t_B from (4.19), for which, with $h_{3_0} = 0.5$, $t_B < 0$ for all relevant values of h_{2_0} (i.e., $0.5 < h_{2_0} < 1$).

5. Discussion

In this article we have studied intrusive gravity flows by employing the three-layer shallow-water equations and a weak stratification version of them when considering analytical work.

Numerical results were obtained using MacCormack's method and a detailed study of the flow geometry as a function of density differences among the various fluid layers as well as fractional depth occupied by them. Criteria for the appearance of the rear shock associated with these intrusive gravity flows were explored and it was found that fractional depth occupied by the flow played a crucial role. We also found that our weak stratification model provided a good representation of the transition to similarity of the flow in terms of the overtaking of the front shock by the rear one. The similarity solutions obtained for both the sudden release of a fixed volume and steady injection were in good agreement with the numerical solutions of the shallow-water equations apart from the fact that they did not reproduce the N-wave visible in Figure 9.

Owing to the importance of bore formation in gravity flows we employed a wavefront expansion technique both to determine conditions under which waves break and to obtain our estimate of the breaking time. This approach allowed for the detection of linear degeneracies associated with the characteristic fields. These degeneracies were shown to have an effect on bore formation.

References

1. J. E. Simpson, *Gravity Currents: In the Environment and the Laboratory*, Ellis Horwood, 1987.
2. R. T. Bonnecaze, H. E. Huppert, and J. R. Lister, Particle-driven gravity currents, *J. Fluid Mech.* 250:339–369 (1993).
3. R. T. Bonnecaze, M. A. Hallworth, H. E. Huppert, and J. R. Lister, Axisymmetric particle-driven gravity currents, *J. Fluid Mech.* 294:93–121 (1995).
4. T. von Kármán, The engineer grapples with nonlinear problems, *Bull. Am. Math. Soc.* 46:615–683 (1940).

5. T. B. Benjamin, Gravity currents and related phenomena, *J. Fluid Mech.* 31:209–248 (1968).

6. G. H. Keulegan, The motion of saline fronts in still water, Nat. Bur. Stand. Report 5831 (1958).

7. D. P. Hoult, Oil spreading on the sea, *Annu. Rev. Fluid Mech.* 4:341–368 (1972).

8. Huppert, 1982.

9. J. W. Rottman and J. E. Simpson, Gravity currents produced by instantaneous releases of a heavy fluid in a rectangular channel, *J. Fluid Mech.* 135:94–110 (1983).

10. S. J. D. D'Alessio, T. B. Moodie, J. P. Pascal, and G. E. Swaters, Gravity currents produced by sudden release of a fixed volume of heavy fluid, *Stud. Appl. Math.*, to appear (1995).

11. R. E. Grundy and J. W. Rottman, The approach to self-similarity of the solutions of the shallow-water equations representing gravity-current releases, *J. Fluid Mech.* 156:39–53 (1985).

12. J. Pedlosky, *Geophysical Fluid Dynamics*, Springer-Verlag, 1987.

13. R. Le Veque, *Numerical Methods for Conservation Laws*, Birkhäuser, 1992.

14. A. Lapidus, A detached shock calculation by second-order finite differences, *J. Comp. Physics* 2:154–177 (1967).

15. T. K. Fannelop and G. D. Waldman, Dynamics of oil slicks, *AIAAJ.* 10:506–510 (1972).

16. G. B. Whitham, *Linear and Nonlinear Waves*, Wiley, 1974.

17. B. R. Seymour and M. P. Mortell, Nonlinear geometrical acoustics, in *Mechanics Today* (S. Nemat-Nasser, Ed.), Vol. 2, pp. 251–312, Pergamon, New York, 1975.

18. T. B. Moodie, Y. He, and D. W. Barclay, Wavefront expansions and nonlinear hyperbolic waves, *Wave Motion* 14:347–367 (1991).

19. P. D. Lax, *Hyperbolic Systems of Conservation Laws and the Mathematical Theory of Shock Waves*, SIAM (1972).

20. Y. He and T. B. Moodie, The signaling problem in nonlinear hyperbolic wave theory, *Stud. Appl. Math.* 85:343–372 (1991).

University of Alberta, Edmonton

(Received October 31, 1995)